

UAV-DETR: Efficient End-to-End Object Detection for Unmanned Aerial Vehicle Imagery

Huaxiang Zhang, Kai Liu, Zhongxue Gan*, and Guo-Niu Zhu*, *Member, IEEE*

Abstract—Unmanned aerial vehicle object detection (UAV-OD) has been widely used in various scenarios. However, most existing UAV-OD algorithms rely on manually designed components, which require extensive tuning. End-to-end models that do not depend on such manually designed components are mainly designed for natural images, which are less effective for UAV imagery. To address such challenges, this paper proposes an efficient detection transformer (DETR) framework tailored for UAV imagery, i.e., UAV-DETR. The framework includes a multi-scale feature fusion with frequency enhancement module, which captures both spatial and frequency information at different scales. In addition, a frequency-focused down-sampling module is presented to retain critical spatial details during down-sampling. A semantic alignment and calibration module is developed to align and fuse features from different fusion paths. Experimental results demonstrate the effectiveness and generalization of our approach across various UAV imagery datasets. On the VisDrone dataset, our method improves AP by 3.1% and AP₅₀ by 4.2% over the baseline. Similar enhancements are observed on the UAVVaste dataset. The project page: <https://github.com/ValiantDiligent/UAV-DETR>

I. INTRODUCTION

Camera-equipped unmanned aerial vehicles (UAVs) have been widely applied in various fields [1]. As one of the core technologies in these applications, UAV object detection (UAV-OD) has attracted considerable attention [2]. Popular UAV-OD algorithms often rely on manually designed components, such as non-maximum suppression (NMS) and anchor boxes generated based on human expertise [3]. These components require extensive tuning for different tasks, which are complex and inefficient in practical applications. In contrast, end-to-end models are free from these issues. Therefore, it would be a good choice to develop end-to-end models for UAV-OD.

As a popular end-to-end model, the Detection Transformer (DETR) [4] utilizes the transformer architecture to create an end-to-end detector. Recent studies have improved the small object detection capabilities of DETR models, but their high computational cost and poor real-time performance make them unsuitable for real-time scenarios [5]. To tackle such issues, Zhao et al. [6] introduced a real-time detection transformer (RT-DETR), which surpassed the popular you only look once (YOLO) framework in both accuracy and speed. However, existing DETRs are predominantly designed

for natural images, which poses challenges when applied to UAV image analysis.

As shown in Fig. 1, the object features in UAV vision are more complex than those in normal vision. Aerial imagery suffers from challenges such as small object sizes and occlusion. Therefore, detecting objects in UAV images typically benefits from detailed feature extraction [2]. In cases where local features may not provide sufficient information, incorporating the relationship between the object and its surrounding environment would be a viable option to enhance the detection accuracy [3], [7].

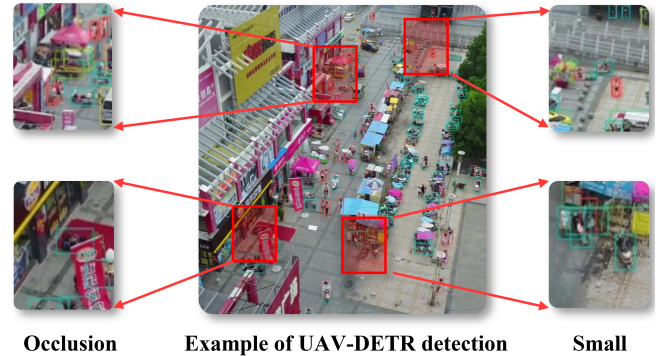


Fig. 1. Challenges in UAV-OD

To handle the challenge of object detection in aerial imagery, this paper proposes an efficient detection transformer framework for UAV imagery, namely UAV-DETR. We enhance our model by leveraging both spatial and frequency domain information across multiple scales to retain high-frequency components. We present a frequency-focused down-sampling strategy to preserve critical spatial details during down-sampling. Finally, we enhance the semantic representation capability of the model by aligning features from different feature fusion paths.

Our main contributions are summarized as follows.

- 1) We propose UAV-DETR, an efficient end-to-end detector transformer for UAV imagery. The framework achieves superior accuracy and real-time performance.
- 2) We present a multi-scale feature fusion with frequency enhancement module to enhance the detection of small and occluded objects.
- 3) We develop a frequency-focused down-sampling module that retains dual-domain information.
- 4) We propose a semantic alignment and calibration module to align features that from different feature fusion paths to boost detection performance.

*This work is supported by Shanghai Municipal Science and Technology Major Project under Grant 2021SHZDZX0103 and Key Project of Comprehensive Prosperity Plan of Fudan University under Grant XM06231744. (Corresponding author: Zhongxue Gan and Guo-Niu Zhu)

All authors are with the Academy for Engineering and Technology, Fudan University, Shanghai 200433, China (e-mail: guoniu.zhu@fudan.edu.cn).

II. RELATED WORK

A. Object Detection in UAV Imagery

Object detection in UAV imagery presents unique challenges, particularly in detecting small objects and managing occlusions. Moreover, UAV-OD often needs to be deployed on hardware platforms, which requires to balance between real-time performance and computational complexity [3]. Some studies [8], [9] presented a coarse-to-fine processing pipeline for UAV-OD. Although these two-stage methods achieve high accuracy, they introduce significant computational overhead [10], which makes them unsuitable for resource-limited environments. To address this issue, another strategy focused on developing optimized single-stage models to balance between detection accuracy and efficiency. Meanwhile, lots of works [2], [11] suggested to capture more features relevant for detecting small objects, with most of them concentrating on utilizing higher-resolution feature maps. In addition, some methods [12], [13] leveraged contextual information to enhance small object detection.

Among these studies, most UAV-OD methods are devoted to lightweighting models or optimizing the processing pipeline for practical use. There is limited research on post-processing techniques. Additionally, these methods mainly extract detailed features and contextual information in the spatial domain, while the frequency domain is underutilized.

B. Real-Time End-to-End Object Detection

Many single-stage UAV-OD models are based on the YOLO series models due to their balance of performance and real-time capability [11], [13]. However, these detectors typically require NMS for post-processing, which not only slows down inference but also introduces hyperparameters that can lead to instability in speed and accuracy.

By contrast, RT-DETR [6] is the first real-time and end-to-end object detector, which eliminates the influence of NMS. It surpasses even the most powerful YOLO models in both speed and accuracy through attention-based intra-scale feature interaction, CNN-based cross-scale feature fusion, and uncertainty-minimal query selection.

RT-DETR leverages global attention mechanisms to capture long-range dependencies and contextual information, which make it more flexible and effective. Its end-to-end design strategy enables it more suitable for deployment on UAV platforms compared to the YOLO series models.

C. Feature Fusion

Feature fusion techniques aim to combine multi-scale feature maps to improve object detection. However, semantic gaps between features at different levels pose challenges, especially for detecting small and densely distributed objects [14]. An intuitive approach is to sum or concatenate feature maps from different layers, though it often leads to spatial feature misalignment. For example, Li et al. [15] presented pooling-based and sampling-based attention mechanisms to investigate these issues.

While these methods focus on spatial feature fusion, the frequency-domain information is not taken into consideration. Although some works [16], [17] explored frequency-domain fusion, they fall short in effective multi-scale fusion across both spatial and frequency domains.

In contrast, our UAV-DETR, a single-stage model with a DETR-like architecture, performs multi-scale feature fusion in both spatial and frequency domains. By using learned offsets to align features across different fusion paths, our approach addresses the misalignment issue and enhances detection performance.

III. METHODOLOGY

As shown in Fig. 2, this study proposes a UAV-DETR, which is built upon the architecture of RT-DETR [6]. We enhance the model with three components, i.e., multi-scale feature fusion with frequency enhancement, frequency-focused down-sampling, and semantic alignment and calibration. Additionally, we introduce inner Scylla intersection over union (Inner-SIoU) [18], [19] to replace the generalized intersection over union (GIoU).

A. Multi-Scale Feature Fusion with Frequency Enhancement

In traditional feature fusion, high-frequency components are often lost. In this study, we present a multi-scale feature fusion with frequency enhancement module (MSFF-FE) to preserve small object details by combining spatial and frequency domain information across multiple scales.

As depicted in Fig. 3, the MSFF-FE adopts a cross stage partial strategy [20]. It partitions the input feature map $x \in \mathbb{R}^{C \times H \times W}$ into two parts: $x_1 \in \mathbb{R}^{C_1 \times H \times W}$ and $x_2 \in \mathbb{R}^{C_2 \times H \times W}$, where $C_1 = \frac{C}{4}$ and $C_2 = \frac{3C}{4}$. The first part x_1 undergoes multi-scale and frequency enhancement, while the second part x_2 is concatenated with the processed features from x_1 , followed by a 1×1 convolution to fuse the two branches. Firstly, the feature map x_1 passes through a 1×1 convolution to adjust its channel dimensions, followed by the GELU activation function [21] for non-linearity, resulting in x_{conv} . Then, frequency domain enhancement is applied using a global average pooling (GAP) operation, followed by a Fourier Transform and an inverse Fourier Transform.

$$x_{sp} = |IF(\text{Conv}_{1 \times 1}(\text{GAP}(x_{conv})) \cdot F(x_{conv}))| \quad (1)$$

To capture multi-scale information, three convolutions with different kernel sizes are applied to x_{sp} .

$$x_{sc} = \text{Conv}_{1 \times 1}(x_{sp}) + \text{Conv}_{3 \times 3}(x_{sp}) + \text{Conv}_{5 \times 5}(x_{sp}) \quad (2)$$

The multi-scale features x_{sc} are further refined by applying a channel attention mechanism. To enhance frequency-based details, we leverage the gating mechanism to modulate and refine the multi-scale features.

$$x_F = \alpha \cdot IF(F(\text{Conv}_{1 \times 1}(x_{sc})) \cdot \text{Conv}_{1 \times 1}(x_{sc})) + \beta \cdot x_{sc} \quad (3)$$

where α and β are learned parameters balancing the spatial and frequency components. We refer to this equation as the frequency-focused module, which will be used in later stages

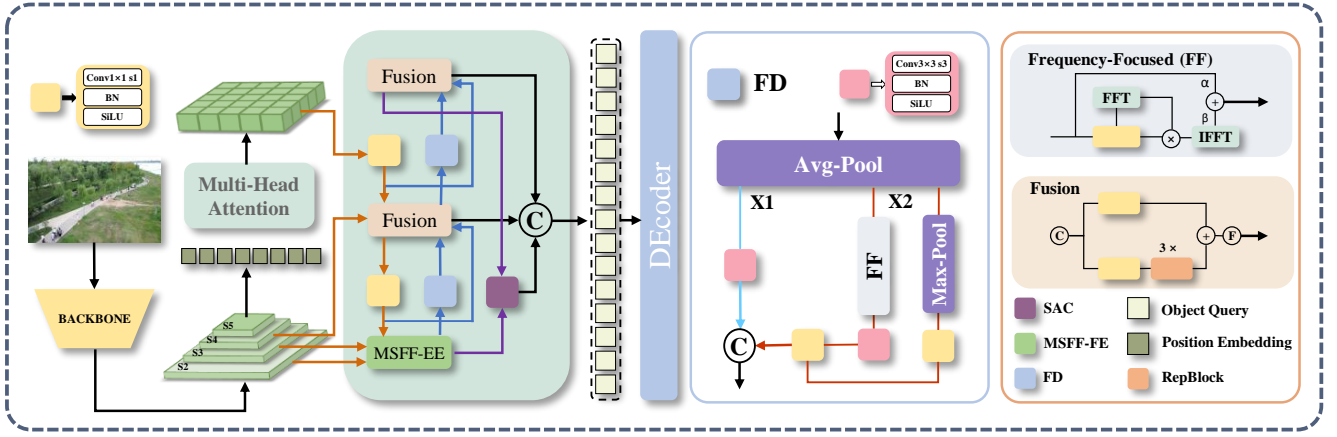


Fig. 2. Overview of the UAV-DETR. MSFF-FE represents the multi-scale feature fusion with frequency enhancement module; FD denotes frequency-focused down-sampling; SAC is semantic alignment and calibration. FFT and IFFT denote fast Fourier transform and its inverse operation, respectively.

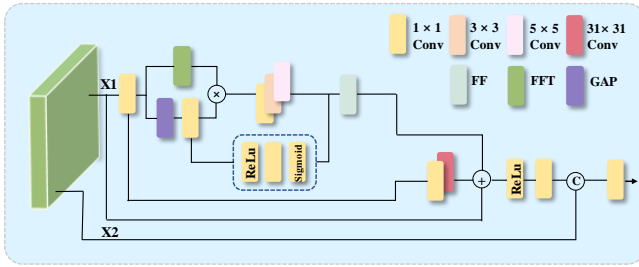


Fig. 3. Structure of multi-scale feature fusion with frequency enhancement.

of the network. Before combining with the unprocessed x_2 , the enhanced features undergo final fusion.

$$x_{\text{final}} = x_1 + \text{Conv}_{31 \times 31}(x_{\text{conv}}) + \text{Conv}_{1 \times 1}(x_{\text{conv}}) + x_F \quad (4)$$

The final output is obtained by concatenating x_{final} with x_2 , followed by a 1×1 convolution.

B. Frequency-Focused Down-Sampling

As illustrated in Fig. 2, in the frequency-focused down-sampling module (FD), the input feature map $x \in \mathbb{R}^{C \times H \times W}$ is first down-sampled using average pooling with a kernel size of 2 and a stride of 1. As a result, the pooled feature map x_p is obtained and then it is divided into two parts: x_1 and x_2 . Each of them are processed in parallel.

x_1 is processed using a 3×3 convolution with stride 2 and padding 1, which reduces its spatial dimensions while preserving key features. Then, x'_1 is obtained. x_2 undergoes parallel processing, where one path applies frequency-focused module to enhance important feature components. Accordingly, x_f is obtained. The other path applies max pooling with a 3×3 kernel and stride 2, followed by a 1×1 convolution to reduce the number of channels. Correspondingly, we get x'_p . The two outputs, x_f and x'_p , are concatenated along the channel dimension and passed through a 1×1 convolution to reduce the number of channels to the desired size, which results in x'_2 . Finally, x'_1 and x'_2 are concatenated to form the final output of the module.

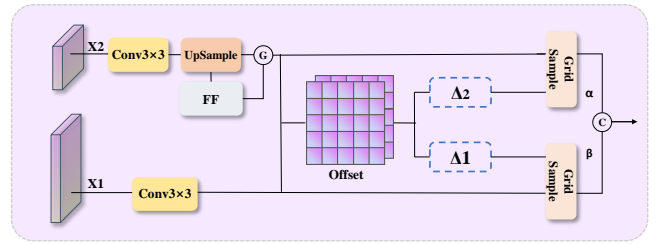


Fig. 4. Structure of semantic alignment and calibration.

C. Semantic Alignment and Calibration

As shown in Fig. 4, the semantic alignment and calibration (SAC) module is designed to fuse and align features obtained from different fusion processes.

Given two input features $x_1 \in \mathbb{R}^{C_1 \times H_1 \times W_1}$ and $x_2 \in \mathbb{R}^{C_2 \times H_2 \times W_2}$, the SAC module first unifies the number of channels to a common dimension C through separate convolution layers. Then, the feature x_2 is upsampled using bilinear interpolation to match the spatial dimensions of x_1 . To enhance feature x_2 , we apply the frequency-focused module, which selectively amplifies high-frequency components. It generates a frequency-enhanced feature x_{freq} . Afterward, we fuse the frequency-enhanced feature with the original upsampled feature x_2 . A gating mechanism is employed to balance the contributions from both the spatial and frequency domains.

$$x_{\text{fused}} = G(x_2) \cdot x_{\text{freq}} + (1 - G(x_2)) \cdot x_2 \quad (5)$$

where G is a learned gating function, which is used to ensure an adaptive fusion of spatial and frequency-domain information.

To address misalignment between x_1 and x_{fused} , the SAC module learns 2D offsets Δ_1 and Δ_2 , which adjust the sampling grid for each feature map. These offsets are generated through a convolutional layer. Using the learned offsets, we adjust the spatial coordinates of the features through a grid-based sampling operation [22] to ensure the alignment of

both features.

$$x_1^{\text{aligned}} = \text{GridSample}(x_1, \Delta_1), \quad (6)$$

$$x_{\text{fused}}^{\text{aligned}} = \text{GridSample}(x_{\text{fused}}, \Delta_2) \quad (7)$$

Then, an element-wise weighted summation is used to fuse the aligned features, where α_1 and α_2 are learned attention weights that balance the contributions from each aligned feature.

$$x_{\text{output}} = \alpha_1 \cdot x_1^{\text{aligned}} + \alpha_2 \cdot x_{\text{fused}}^{\text{aligned}} \quad (8)$$

D. LOSS Function

RT-DETR uses GIoU loss for bounding box regression, which is less effective for small object detection, especially when the Intersection over Union (IoU) values are low. To address this issue, we adopt Inner-SIoU, which enhances both small object detection and geometric alignment. Inner-SIoU combines Inner-IoU [19] and SCYLLA-IoU (SIoU) [18]. It scales the auxiliary bounding box by 1.25 to improve sensitivity and speed up convergence. Like SIoU, it adds angle and shape losses to reduce angular and distance mismatches.

The InnerIoU is defined using expanded auxiliary bounding boxes. For a given predicted box B^{inner} and ground truth box $B_{\text{gt}}^{\text{inner}}$, the Inner-IoU is calculated as:

$$\text{Inner-IoU} = \frac{|B^{\text{inner}} \cap B_{\text{gt}}^{\text{inner}}|}{|B^{\text{inner}} \cup B_{\text{gt}}^{\text{inner}}|} \quad (9)$$

where B^{inner} and $B_{\text{gt}}^{\text{inner}}$ represent the expanded predicted and ground truth boxes, respectively. The width and height of both boxes are scaled by a factor of 1.25. The terms $|B^{\text{inner}} \cap B_{\text{gt}}^{\text{inner}}|$ and $|B^{\text{inner}} \cup B_{\text{gt}}^{\text{inner}}|$ denote the area of overlap and the union area between the expanded boxes, respectively.

The Inner-SIoU loss is defined as:

$$L_{\text{Inner-SIoU}} = L_{\text{SIoU}} + \text{IoU} - \text{Inner-SIoU} \quad (10)$$

where IoU is the standard IoU loss, and L_{SIoU} includes angle, distance, and shape penalties.

IV. EXPERIMENTS

A. Experimental Setup

Datasets: We conduct quantitative experiments on two object detection datasets: VisDrone [23] and UAVVaste [24]. The VisDrone-2019-DET dataset comprises 6,471 training images, 548 validation images, and 3,190 test images, all captured from drones at varying altitudes across different locations. Each image is annotated with bounding boxes for ten predefined object categories: pedestrian, person, car, van, bus, truck, motorbike, bicycle, awning-tricycle, and tricycle. We used the VisDrone-2019-DET training set and validation set for training and testing, respectively.

In addition, we further train the UAV-DETR network with UAVVaste dataset to validate the capacity to generalize across datasets. UAVVaste is a dataset designed specifically for aerial rubbish detection. It consists of 772 images and 3716 hand-labeled annotations of waste in urban and natural

environments such as streets, parks, and lawns. We choose the training set for training and the test set for testing.

Implementation Details: All models are trained on NVIDIA GeForce RTX 3090. For the details of the network architecture, our UAV-DETR model is based on RT-DETR [6], with two model sizes designed: one using ResNet18 and the other using ResNet50 as the backbone. We implement our approach and train the framework for 400 epochs with a batch size of 4. We use an early stopping mechanism with a patience setting of 20. The UAV-DETR network is optimized using AdamW [25] with a learning rate of 0.0001, a momentum of 0.9. We scale our input images to 640×640 pixels and use the data augmentation methods from the RT-DETR model to ensure consistency across experiments. Additionally, we apply mixup [26] and Mosaic [27] techniques, with Mosaic set to a probability of 1 and mixup set to a probability of 0.2. We report the standard COCO metrics, including AP (averaged over uniformly sampled IoU thresholds ranging from 0.50-0.95 with a step size of 0.05), and AP₅₀ (AP at an IoU threshold of 0.50).

B. Comparative Experiments

As listed in Table I, on the VisDrone dataset, our UAV-DETR-R18 achieves a 3.1% improvement in AP, a 4.2% increase in AP₅₀ compared to the baseline RT-DETR-R18. Similarly, the UAV-DETR-R50 sees a 3.1% increase in AP, a 4.1% rise in AP₅₀ compared to the baseline. UAV-DETR-R18 outperforms all methods with a computational cost below 100 GFLOPs, achieving the best accuracy in its class. Furthermore, we compared our method with other object detectors that have similar computational costs to UAV-DETR-R50, and the results show that our approach also outperforms the others in terms of accuracy. Remarkably, our method still exhibits outstanding performance, even compared to approaches like PP-YOLOE-P2-Alpha-1 [28], which typically benefit from extensive pre-training. Such comparisons are often considered unfair due to the significant advantages conferred by extensive pre-training.

To further demonstrate the generalization ability of UAV-DETR, we also evaluated the method on the UAVVaste dataset. UAV-DETR-R18 was chosen for this comparison as it strikes an optimal balance between computational efficiency and detection accuracy, making it well-suited for evaluation on a smaller dataset like UAVVaste, where maintaining strong performance with limited data is crucial. The compared methods were implemented using the ultralytics toolkits [29], and the results are shown in Table II. Notably, UAV-DETR still maintains a competitive advantage compared to other models, with an improvement of 3.3% and 3.6% in AP and AP₅₀, respectively, compared to the baseline. The results indicate that the proposed method is both feasible and effective for detecting objects in drone images. Compared to VisDrone, the UAVVaste dataset has a smaller amount of data. The strong performance of our model demonstrates that it does not rely on large amounts of annotated data.

TABLE I
EXPERIMENTAL RESULTS ON THE VISDRONE-2019-DET DATASET

Model	Publication	InputSize	Params(M)	GFLOPs	AP	AP ₅₀
<i>Real-time Object Detectors</i>						
YOLOv8-M [29]	-	640×640	25.9	78.9	24.6	40.7
YOLOv8-L [29]	-	640×640	43.7	165.2	26.1	42.7
YOLOv9-M [30]	arXiv2024	640×640	20.1	76.8	25.2	42.0
YOLOv10-M [31]	arXiv2024	640×640	15.4	59.1	24.5	40.5
YOLOv10-L [31]	arXiv2024	640×640	24.4	120.3	26.3	43.1
<i>Object Detectors for UAV Imagery</i>						
PP-YOLOE-P2-Alpha-1 [28]	-	640×640	54.1	111.4	30.1	48.9
QueryDet [8]	CVPR2022	2400×2400	33.9	212	28.3	48.1
ClusDet [9]	ICCV2019	1000×600	30.2	207	26.7	50.6
DCFL [32]	CVPR2023	1024×1024	36.1	157.8	-	32.1
DetectoRS w/ RFLA [33]	ECCV2022	800×800	123.2	160	27.4	45.3
HIC-YOLOv5 [2]	ICRA2024	640×640	9.4	31.2	20.8	36.1
<i>End-to-end Object Detectors</i>						
DETR [4]	ECCV2020	1333×750	60	187	24.1	40.1
Deformable DETR [5]	ICLR2020	1333×800	40	173	27.1	42.2
Sparse DETR [34]	ICLR2022	1333×800	40.9	121	27.3	42.5
RT-DETR-R18 [6]	CVPR2024	640×640	20	60.0	26.7	44.6
RT-DETR-R50 [6]	CVPR2024	640×640	42	136	28.4	47.0
<i>Real-time End-to-end Object Detectors for UAV Imagery</i>						
UAV-DETR-R18(Ours)	-	640×640	20	77	29.8	48.8
UAV-DETR-R50(Ours)	-	640×640	42	170	31.5	51.1

TABLE II
EXPERIMENTAL RESULTS ON UAVASTE DATASET

Model	AP	AP ₅₀
HIC-YOLOv5 [2]	40.5	66.8
YOLOv8-M [29]	40.5	68.6
RT-DETR [6]	42.4	71.1
UAV-DETR(Ours)	45.7	74.7

TABLE III
RESULTS OF THE ABLATION STUDY.

Baseline	IS	MSFF-FE	FD	SAC	AP	AP ₅₀
✓					26.7	44.6
✓	✓				27.1	45.3
✓	✓	✓			28.4	46.9
✓	✓	✓	✓		28.4	47.1
✓	✓	✓		✓	28.9	47.7
✓	✓	✓	✓	✓	29.8	48.8

C. Ablation Studies

We conducted ablation experiments on the VisDrone dataset using UAV-DETR-R18 to analyze the impact of each component on detection accuracy. Table III presents the performance comparison with different configurations, where IS stands for Inner-SIoU, MSFF-FE represents Multi-Scale Feature Fusion with Frequency Enhancement module, FD stands for Frequency-Focused Down-Sampling module, and SAC refers to Semantic Alignment and Calibration module.

TABLE IV
COMPARISON OF IOU METRICS

IoU	AP	AP ₅₀
GIoU	29.0	48.4
Inner-SIoU (ratio=1.20)	29.5	48.7
Inner-SIoU (ratio=1.25)	29.8	48.8
Inner-SIoU (ratio=1.30)	29.3	48.6

TABLE V
COMPARISON OF MODEL PERFORMANCE METRICS

Model	Params(M)	GFLOPs	FPS
RT-DETR-R18 [6]	20	60	85
RT-DETR-R50 [6]	42	130	40
UAV-DETR-R18	20	77	51
UAV-DETR-R50	42	170	30

The baseline RT-DETR-R18 achieves an AP of 26.7 and AP₅₀ of 44.6. After incorporating Inner-SIoU, AP increased to 27.1, showing that improving the loss function positively impacts performance. Adding the MSFF-FE module further improves the AP to 28.4, demonstrating the benefits of incorporating multi-scale feature fusion and frequency enhancement. The addition of FD improves AP₅₀, reaching 47.1. Incorporating the SAC module results in further gains, with AP reaching 28.9 and AP₅₀ improving to 47.7. When all components are combined, UAV-DETR-R18 achieves the highest performance with an AP of 29.8 and an AP₅₀ of 48.8, showcasing the cumulative impact of each module on detection accuracy. As shown in Table IV, our experiments demonstrate that setting the ratio of Inner-SIoU to 1.25 is an appropriate choice. Lastly, we calculated the Frames Per Second (FPS) for both the baseline and UAV-DETR models using the PyTorch implementation in 32-bit Floating Point Precision, as shown in Table V. The results show that UAV-DETR is capable of meeting real-time requirements.

D. Visualization

In Fig. 5, we present heatmaps for small objects in the VisDrone dataset, focusing on backpropagation through the bounding box predictions. Compared to the baseline model, UAV-DETR demonstrates a notably improved ability to localize small objects. In the heatmaps of our model, small objects exhibit higher heat values, indicating that the

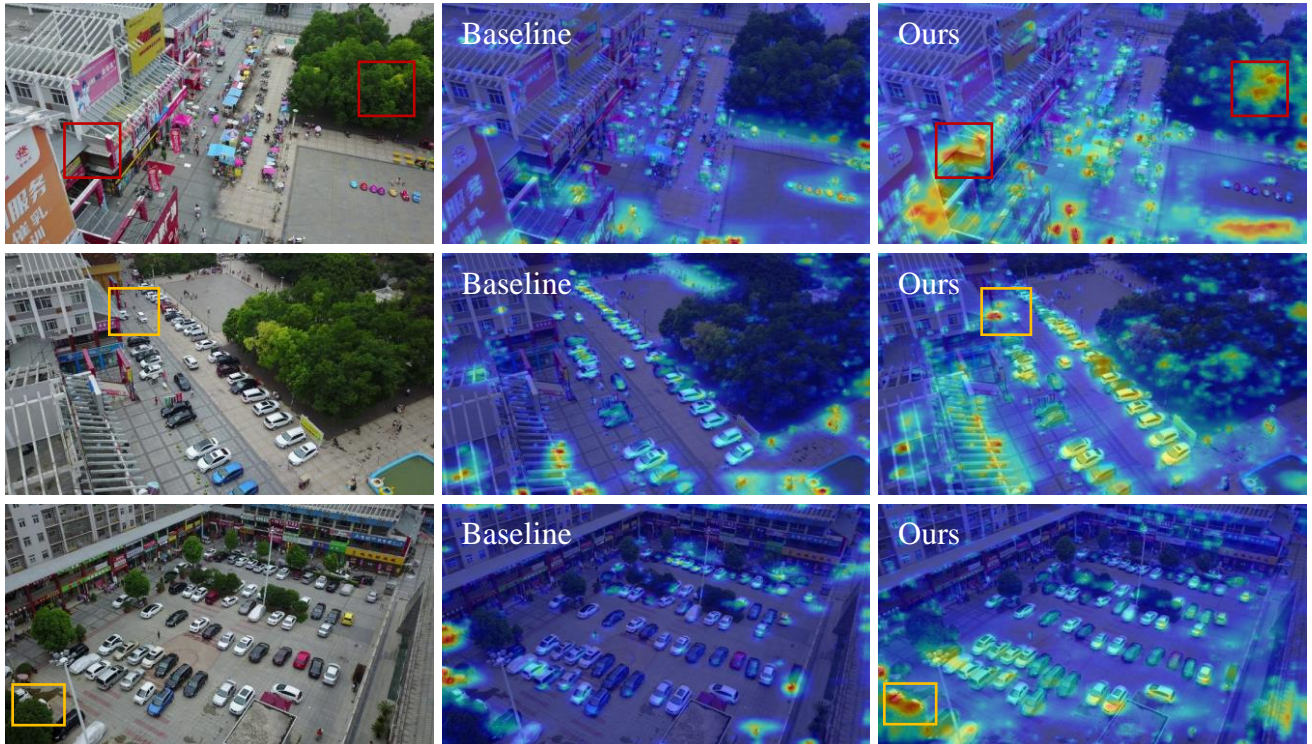


Fig. 5. The heatmap of RT-DETR-R18 and UAV-DETR-R18. The brighter areas in the heatmap indicate stronger attention by the model. Our model shows greater focus on small objects and their surrounding environment. The yellow boxes highlight areas where our model performs better in detecting occluded objects. The red boxes indicate regions where the model misfocuses on noise.

model can more effectively capture the features of these small objects. Additionally, it can be observed that UAV-DETR pays more attention to the surrounding information of small objects, demonstrating the model’s ability to better utilize contextual information during detection. As a result, as shown in the yellow box in Fig. 5, UAV-DETR also performs well in localizing occluded objects.

E. Discussion

Compared to other UAV-OD models, UAV-DETR has two key differences. First, it eliminates the need for NMS and anchor setting, which greatly reduces the complexity of model deployment. Second, UAV-DETR leverages dual-domain information during feature fusion. As shown in Table I, our model achieves higher accuracy compared to other detectors with similar computational costs.

There are several reasons that contribute to this improved performance. Firstly, our model retains more high-frequency features, which are crucial for detecting small objects. In traditional feature fusion and down-sampling processes, high-frequency features are often lost, making it harder to recover edge and texture details. These details are particularly important for UAV-OD. To address this, we introduced the MSFF-FE and FD modules, which enable the model to combine spatial and frequency domain information during both feature fusion and down-sampling, ensuring that important high-frequency components are preserved.

Secondly, our model makes better use of contextual information. When small objects are difficult to detect based

on fine details, their surrounding semantic context becomes crucial. The operations in the frequency domain help the model capture global patterns, improving detection accuracy. However, these operations can sometimes lead to misalignment between the semantic and spatial information of different feature maps. To address this, we designed the SAC module, which aligns features from different fusion paths and enhances overall detection performance. The ablation study in Table III supports the effectiveness of these modules.

Our findings suggest that utilizing frequency domain information can enhance the performance of UAV-OD. We hope this approach will provide insights into how frequency information can be better used in UAV-OD tasks. However, as shown in the red box in Fig. 5, the model occasionally focuses on irrelevant regions, which presents a challenge that we aim to address in future work.

V. CONCLUSION

We design UAV-DETR, a real-time end-to-end object detector specifically designed for UAV imagery. By introducing the MSFF-FE module, FD module, and SAC module, UAV-DETR helps alleviate the difficulties of detecting small and occluded objects in aerial images. Experimental results on the VisDrone and UAVVaste datasets demonstrate that our method achieves higher accuracy than existing approaches with similar computational costs, all while maintaining real-time inference speeds. Future work will focus on improving its robustness to noise.

REFERENCES

- [1] B. Wang, W. Li, B. Zhang, and Y. Liu, "Joint response and background learning for uav visual tracking," in *2024 IEEE International Conference on Robotics and Automation (ICRA)*, 2024, pp. 455–462.
- [2] S. Tang, S. Zhang, and Y. Fang, "Hic-yolov5: Improved yolov5 for small object detection," in *2024 IEEE International Conference on Robotics and Automation (ICRA)*. IEEE, 2024, pp. 6614–6619.
- [3] K. Tong, Y. Wu, and F. Zhou, "Recent advances in small object detection based on deep learning: A review," *Image and Vision Computing*, vol. 97, p. 103910, 2020.
- [4] N. Carion, F. Massa, G. Synnaeve, N. Usunier, A. Kirillov, and S. Zagoruyko, "End-to-end object detection with transformers," in *Computer Vision – ECCV 2020*, A. Vedaldi, H. Bischof, T. Brox, and J.-M. Frahm, Eds. Cham: Springer International Publishing, 2020, pp. 213–229.
- [5] X. Zhu, W. Su, L. Lu, B. Li, X. Wang, and J. Dai, "Deformable detr: Deformable transformers for end-to-end object detection," in *International Conference on Learning Representations*, 2020.
- [6] Y. Zhao, W. Lv, S. Xu, J. Wei, G. Wang, Q. Dang, Y. Liu, and J. Chen, "Detrs beat yolos on real-time object detection," in *Proceedings of the IEEE/CVF Conference on Computer Vision and Pattern Recognition (CVPR)*, June 2024, pp. 16965–16974.
- [7] Y. Li, Q. Hou, Z. Zheng, M.-M. Cheng, J. Yang, and X. Li, "Large selective kernel network for remote sensing object detection," in *Proceedings of the IEEE/CVF International Conference on Computer Vision (ICCV)*, October 2023, pp. 16 794–16 805.
- [8] C. Yang, Z. Huang, and N. Wang, "Querydet: Cascaded sparse query for accelerating high-resolution small object detection," in *Proceedings of the IEEE/CVF Conference on Computer Vision and Pattern Recognition (CVPR)*, June 2022, pp. 13 668–13 677.
- [9] F. Yang, H. Fan, P. Chu, E. Blasch, and H. Ling, "Clustered object detection in aerial images," in *Proceedings of the IEEE/CVF International Conference on Computer Vision*, 2019, pp. 8311–8320.
- [10] J. Feng, J. Wang, and R. Qin, "Lightweight detection network for arbitrary-oriented vehicles in uav imagery via precise positional information encoding and bidirectional feature fusion," *International Journal of Remote Sensing*, vol. 44, no. 15, pp. 4529–4558, 2023.
- [11] P. Mittal, R. Singh, and A. Sharma, "Deep learning-based object detection in low-altitude uav datasets: A survey," *Image and Vision Computing*, vol. 104, p. 104046, 2020.
- [12] C. Shen, C. Ma, and W. Gao, "Multiple attention mechanism enhanced yolox for remote sensing object detection," *Sensors*, vol. 23, no. 3, p. 1261, 2023.
- [13] Y. Liu, P. Sun, N. Wergeles, and Y. Shang, "A survey and performance evaluation of deep learning methods for small object detection," *Expert Systems with Applications*, vol. 172, p. 114602, 2021.
- [14] J. Deng, S. Bei, S. Shaojing, and Z. Zhen, "Feature fusion methods in deep-learning generic object detection: A survey," in *2020 IEEE 9th Joint International Information Technology and Artificial Intelligence Conference (ITAIC)*, vol. 9. IEEE, 2020, pp. 431–437.
- [15] K. Li, Q. Geng, M. Wan, X. Cao, and Z. Zhou, "Context and spatial feature calibration for real-time semantic segmentation," *IEEE Transactions on Image Processing*, vol. 32, pp. 5465–5477, 2023.
- [16] Y. Cui, W. Ren, and A. Knoll, "Omni-kernel network for image restoration," in *Proceedings of the AAAI Conference on Artificial Intelligence*, vol. 38, no. 2, 2024, pp. 1426–1434.
- [17] G. Liu, Z. Chen, D. Liu, B. Chang, and Z. Dou, "Ftmf-net: A fourier transform-multiscale feature fusion network for segmentation of small polyp objects," *IEEE Transactions on Instrumentation and Measurement*, vol. 72, pp. 1–15, 2023.
- [18] Z. Gevorgyan, "Siou loss: More powerful learning for bounding box regression," *arXiv preprint arXiv:2205.12740*, 2022.
- [19] H. Zhang, C. Xu, and S. Zhang, "Inner-iou: more effective intersection over union loss with auxiliary bounding box," *arXiv preprint arXiv:2311.02877*, 2023.
- [20] C.-Y. Wang, H.-Y. M. Liao, Y.-H. Wu, P.-Y. Chen, J.-W. Hsieh, and I.-H. Yeh, "Cspnet: A new backbone that can enhance learning capability of cnn," in *Proceedings of the IEEE/CVF Conference on Computer Vision and Pattern Recognition (CVPR) Workshops*, June 2020.
- [21] D. Hendrycks and K. Gimpel, "Gaussian error linear units (gelus)," *arXiv preprint arXiv:1606.08415*, 2016.
- [22] M. Jaderberg, K. Simonyan, A. Zisserman *et al.*, "Spatial transformer networks," *Advances in neural information processing systems*, vol. 28, 2015.
- [23] P. Zhu, L. Wen, D. Du, X. Bian, H. Fan, Q. Hu, and H. Ling, "Detection and tracking meet drones challenge," *IEEE Transactions on Pattern Analysis and Machine Intelligence*, vol. 44, no. 11, pp. 7380–7399, 2021.
- [24] M. Kraft, M. Piechocki, B. Ptak, and K. Walas, "Autonomous, onboard vision-based trash and litter detection in low altitude aerial images collected by an unmanned aerial vehicle," *Remote Sensing*, vol. 13, no. 5, 2021.
- [25] I. Loshchilov, "Decoupled weight decay regularization," *arXiv preprint arXiv:1711.05101*, 2017.
- [26] H. Zhang, M. Cisse, Y. N. Dauphin, and D. Lopez-Paz, "mixup: Beyond empirical risk minimization," in *International Conference on Learning Representations*, 2018.
- [27] A. Bochkovskiy, C.-Y. Wang, and H.-Y. M. Liao, "Yolov4: Optimal speed and accuracy of object detection," *arXiv preprint arXiv:2004.10934*, 2020.
- [28] P. Authors, "Paddledetection, object detection and instance segmentation toolkit based on paddlepaddle." <https://github.com/PaddlePaddle/PaddleDetection>, 2019.
- [29] G. Jocher, A. Chaurasia, and J. Qiu, "Ultralytics yolov8," 2023. [Online]. Available: <https://github.com/ultralytics/ultralytics>
- [30] C.-Y. Wang and H.-Y. M. Liao, "YOLOv9: Learning what you want to learn using programmable gradient information," *arXiv preprint arXiv:2402.13616*, 2024.
- [31] A. Wang, H. Chen, L. Liu, K. Chen, Z. Lin, J. Han, and G. Ding, "Yolov10: Real-time end-to-end object detection," *arXiv preprint arXiv:2405.14458*, 2024.
- [32] C. Xu, J. Ding, J. Wang, W. Yang, H. Yu, L. Yu, and G.-S. Xia, "Dynamic coarse-to-fine learning for oriented tiny object detection," in *Proceedings of the IEEE/CVF Conference on Computer Vision and Pattern Recognition (CVPR)*, June 2023, pp. 7318–7328.
- [33] C. Xu, J. Wang, W. Yang, H. Yu, L. Yu, and G.-S. Xia, "Rfla: Gaussian receptive field based label assignment for tiny object detection," in *European Conference on Computer Vision*. Springer, 2022, pp. 526–543.
- [34] B. Roh, J. Shin, W. Shin, and S. Kim, "Sparse detr: Efficient end-to-end object detection with learnable sparsity," in *ICLR*, 2022.